Major Scientific Results from SOHO on Coronal Mass Ejections

N. Gopalswamy[1], B. Fleck[1,2] and J. B. Gurman[1]
[1]NASA Goddard Space Flight Center, Greenbelt, MD 20771 USA
[2]European Space Agency

Abstract: Major scientific results related to coronal mass ejections (CMEs) observed by the Solar and heliospheric Observatory (SOHO) mission are discussed. After a brief description of the general properties of CMEs, their relationship to geomagnetic storms, solar energetic particles, and radio bursts is discussed. Also discussed are the CME-driven shocks and their interaction with other CMEs.

1. Introduction

The Solar and Heliospheric Observatory (SOHO) mission was launched on 1995 December 2 carrying a set of 12 instruments on board to acquire information on the interior, surface, and the extended atmosphere of the Sun with unprecedented spatial and temporal resolution (see Table 1). The SOHO mission is a joint project between the European Space Agency (ESA) and the US National Aeronautics and Space Administration (NASA). The spacecraft has been positioned in a halo orbit around the Earth-Sun L1 Lagrangian point (~1.5 million km from Earth) in order to view the Sun continuously and is commanded from NASA's Goddard Space Flight Center (GSFC) in Greenbelt, Maryland. NASA's Deep Space Network (DSN) is used to retrieve the data from the spacecraft at the rate of 200 kb/s. The data are made freely available online as soon as possible. The SOHO data have aided major advances in understanding the sources of solar variability, starting with the solar interior and extending through the corona to the solar wind. Nearly 4000 papers have been published using SOHO data (see http://sohowww.nascom.nasa.gov/publications for a complete list). It is next to impossible to summarize all the results. Instead, we highlight major results pertaining to coronal mass ejections (CMEs), which constitute the most energetic phenomenon in the heliosphere, occasionally affecting the entire heliosphere. CMEs are an important consideration in the planetary exploration activities because the energetic particles and plasmas associated with the CMEs are of immediate concern. SOHO has observed more than 9000 CMEs since the launch in 1995 to the end of 2004. This is an unprecedented data set surpassing the total extent of CME data from all pre-SOHO missions put together. The vast data set has confirmed a number of previous results and produced many surprising new results. We highlight several of these new results.

Table 1 Physical space probed and measurements made by SOHO instruments

Spatial Domain of investigation	Instruments	Measurement
Solar Interior	GOLF	Solar Oscillations (global velocity)
	VIRGO	Solar Oscillations (irradiance)
	MDI/SOI	Surface Oscillations, Photospheric Magnetic field
Solar Atmosphere	SUMER	Physical parameters - inner corona
	CDS	Physical parameters - inner corona
	EIT	Physical parameters - inner corona
	LASCO	Physical parameters - entire corona
	UVCS	Physical parameters - entire corona
Heliosphere (solar wind)	CELIAS	Composition (charge, element, isotope)
	COSTEP	Superthermal and energetic particles
	ERNE	Solar energetic particles
	SWAN	Large-scale solar-wind structures

CDS - Coronal Diagnostic Spectrometer; CELIAS - Charge, Element, and Isotope Analysis System; COSTEP - Comprehensive Suprathermal and Energetic Particle Analyzer; EIT - Extreme ultraviolet Imaging Telescope; ERNE - Energetic and Relativistic Nuclei and Electron experiment; GOLF - Global Oscillations at Low Frequencies; LASCO - Large Angle and Spectrometric Coronagraph; MDI/SOI - Michelson Doppler Imager/Solar Oscillations Investigation; SUMER - Solar Ultraviolet Measurements of Emitted Radiation; SWAN - Solar Wind Anisotropies; UVCS - Ultraviolet Coronagraph Spectrometer; VIRGO Variability of Solar Irradiance and Gravity Oscillations.

2. Coronal Mass Ejections

SOHO's Large Angle and Spectrometric Coronagraph (LASCO, Brueckner et al., 1995) continuously records CMEs over a field of view of 3-32 solar radii (Rs) using its two telescopes C2 and C3. The C1 telescope, which can observe CMEs closer to the Sun was disabled in June 1998. The CME results we present here primarily come from LASCO C2 and C3. CMEs are large-scale magnetized plasma structures ejected from closed field regions on the Sun such as active regions, filament regions, and interconnected active regions. The measured speeds in the sky plane range from tens of km/s to nearly 3000 km/s, with an average value of ~450 km/s (see e.g., (Yashiro et al., 2004; Gopalswamy, 2004a and references therein). The apparent angular width of CMEs ranges from a few degrees to more than 120 degrees, with an average value of ~47 deg (counting only CMEs with width less than 120 deg , but CMEs do occasionally attain very large widths – see Fig. 1). The total mass ejected ranges in CMEs from a few times 10^{13} g to more than 10^{16} g. Accordingly, the kinetic energy of CMEs with angular width <120° ranges from ~10^{27} erg to ~10^{32} erg, with an average value of 5×10^{29} erg. Some very fast and wide CMEs can have kinetic energies exceeding 10^{33} erg, generally originating from large active regions (Gopalswamy et al., 2005a). Most CMEs show some amount of acceleration in the coronagraphic field of view (see Fig. 2). Slow CMEs (<200 km/s) typically accelerate. CMEs moving with speeds close to the slow solar wind (~400 km/s) usually have no acceleration. CMEs exceeding a speed of 400 km/s typically decelerate, with the magnitude proportional to the speed. Most of the CMEs also show acceleration over the Sun-Earth distance (Gopalswamy et al. 2000a; 2001b). CMEs are made of multithermal plasmas: the temperature ranges from ~8000 K in the inner core to a few MK in the outer structure. Occasionally, CMEs may consist of flare ejecta with temperature exceeding 10 MK. The magnetic field in CMEs is not directly measurable, but we can infer structures with a few gauss in the hot coronal structures to tens of gauss in the prominence core.
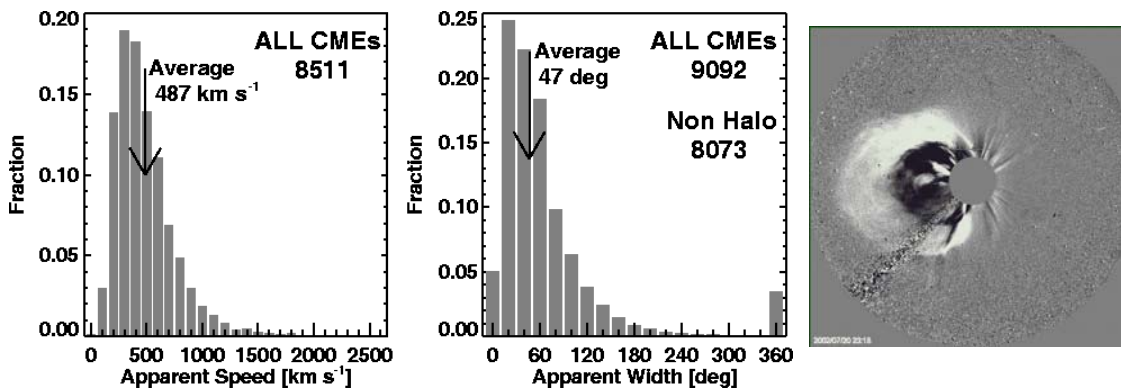

Figure 1. Distribution of CME speeds (left), widths (middle) measured in the sky plane for 1996-2004. A SOHO/LASCO CME originating at the east limb and attaining a width of ~180 deg. The average width was determined using non-halo CMEs because the true width of halo CMEs is unknown (see text).
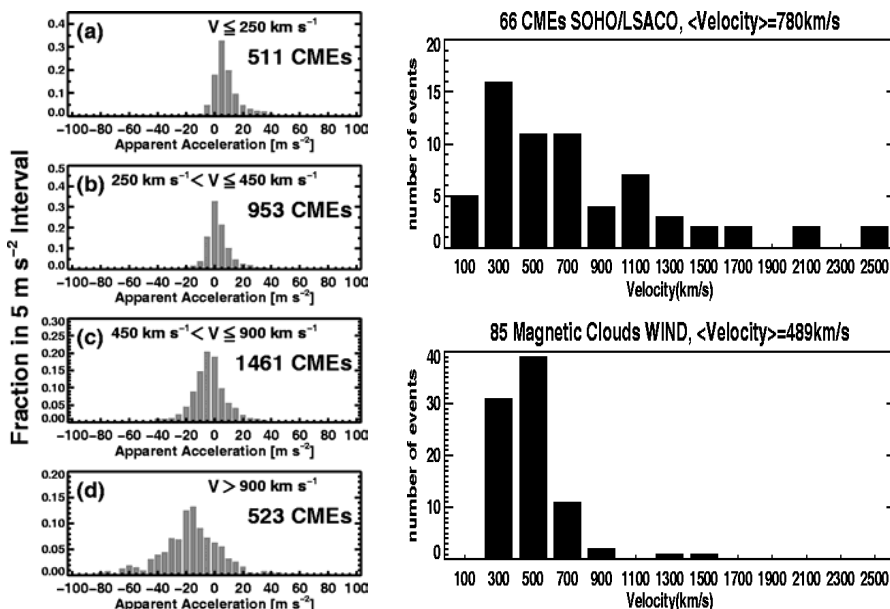

Figure 2. (left) CME acceleration for various speed groups showing more decelerating events as one goes from lower to higher speed groups. (right) comparison between the speed distributions of 66 SOHO/LASCO CMEs that have interplanetary counterparts and 85 magnetic clouds detected at 1 AU. One can see that the magnetic cloud distribution is narrower than that of the SOHO/LSCO CMEs. This happens because slow CMEs accelerate and fast CMEs decelerate.

2

2.1 CME Rate

During solar minima, the CME rate is typically 0.5/day. The rate during solar maxima could be an order of magnitude higher. Figure 3 shows the CME rate averaged over the Carrington Rotation periods (27.3 days) compared with the Sunspot Number (SSN). One of the biggest surprises of SOHO observations has been that the daily CME rate during solar maximum is much higher than the pre-SOHO values. Hildner et al. (1976) had predicted a peak rate of 3.2 CMEs/day based on Skylab data over 7 solar rotations [rate = 0.96+0.084 SSN] (see also Webb and Howard, 1994). SOHO data also confirmed the relationship, but the slope of the regression line is much different, because the peak CME rate exceeded 6/day (Gopalswamy et al., 2003a). The second surprise is that the correlation between the daily CME rate and SSN is also less than perfect, especially for large SSN (near solar maximum). CMEs occurring with a relatively high rate originating from the polar crown filaments (PCFs) around solar maximum have nothing to do with sunspots and hence need not be correlated with SSN. Both SSN and CME rates show a double maximum (late 2000 and early 2002), but the first peak is higher for SSN, while the second peak is higher for the CME rate. The rate of high latitude (HL) CMEs is clearly related to the migration of closed field structures to the poles. Figure 3 shows that the low-latitude (LL) CME rate is generally higher than the HL rate, but occasionally they can be very close. Analyzing the CME rate grouped into HL and LL rates resulted in another important discovery: the cessation of HL CMEs coincided with the polarity reversal at the solar poles (Gopalswamy et al. 2003b). The HL CMEs provide a natural explanation for the disappearance PCFs, which need to be removed before the poles could acquire open field structure of the opposite polarity. This is illustrated by a cartoon in Fig 3.
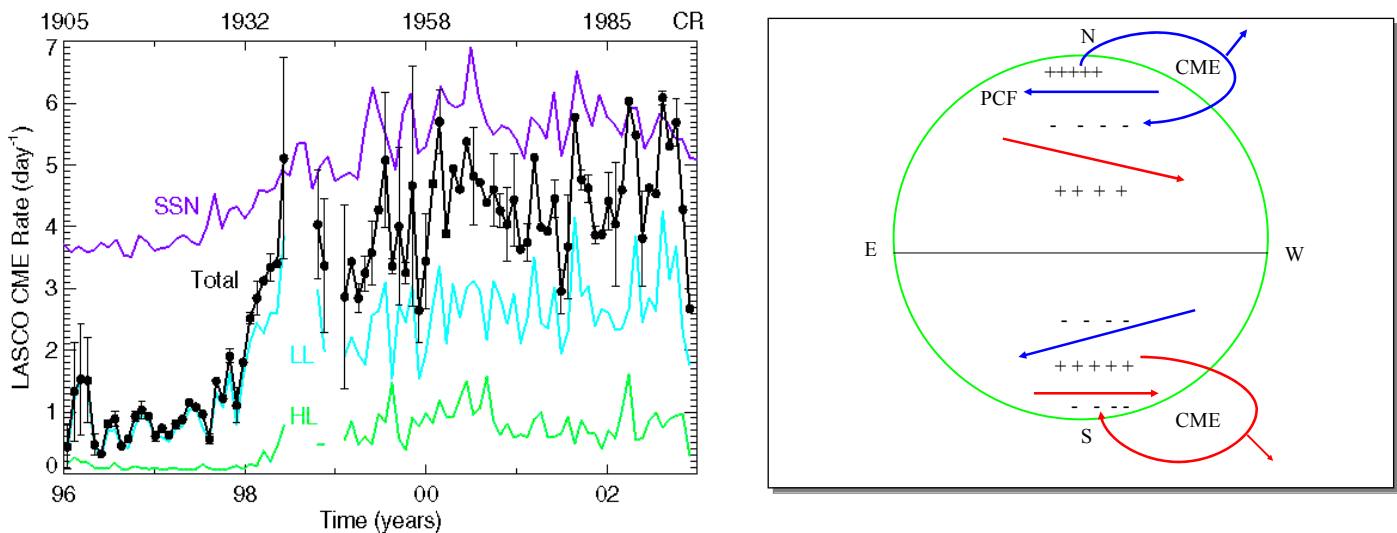

Figure 3. (left) Daily CME rates from high latitudes (HL), low latitudes (LL) and from all latitudes (Total) compared with daily sunspot numbers (SSN). (right) A cartoon showing the general magnetic pattern on the solar surface with the polar crown filaments (PCF) indicated by the horizontal arrows (also representing the axial magnetic field direction in the filaments). The slanted arrows represent the secondary PCF, which become the primary PCF in the next solar cycle. The '+' and '-' symbols indicate the polarities of the photospheric magnetic field. The PCF and the overlying structures need to erupt before the polarity can be reversed.

An interesting consequence of the HL CME rate and polarity reversal is the connection to the modulation of galactic cosmic rays (GCRs). Newkirk et al. (1981) had identified CMEs as the solar origin of the low-frequency power in the interplanetary magnetic field fluctuations and suggested that the solar-cycle dependent modulation of GCRs can be explained by the presence of the fluctuations in the heliosphere. For effective modulation, a higher and more cycle-dependent CME occurrence rate (varying by factors up to 10) was required than pre-SOHO data indicated (Wagner, 1984). SOHO has demonstrated the higher and more cycle-dependent rate (when HL CMEs are considered) and hence the GCR modulation should be possible. It was indeed found that the GCR intensity was (anti)correlated well with the HL CME rate during the rise phase (A>0

epoch) of cycle 23 (Lara et al., 2005). When we looked at the CME from the A<0 epoch of cycle 22 (July 1982 – August 1985) and repeated the analysis again by separating the HL and LL CMEs, we found the opposite was true: the LL CME rate was better (anti)correlated with the GCR intensity (Gopalswamy, 2004a). The switch in the dominant correlation (see Figure 4) is directly linked to the A>0 and A<0 epochs of the solar polar field, which decides how the GCR protons enter the heliosphere resulting in the 22-year pattern of GCR modulation.
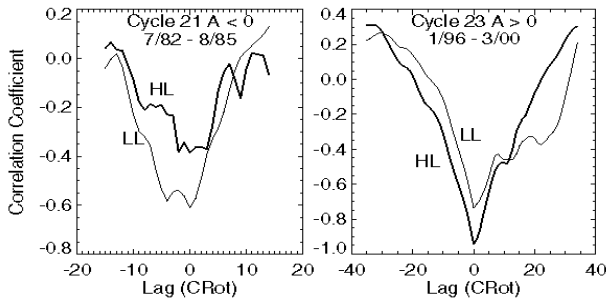

Figure 4. Cross-correlation between GCR intensity and HL and LL CME rates for (left) the A< 0 epoch of cycle 21 and (right) the A>0 epoch of cycle 23. Note the switching of he dominant correlation between cycles 22 (A<0) and 23 (A>0).
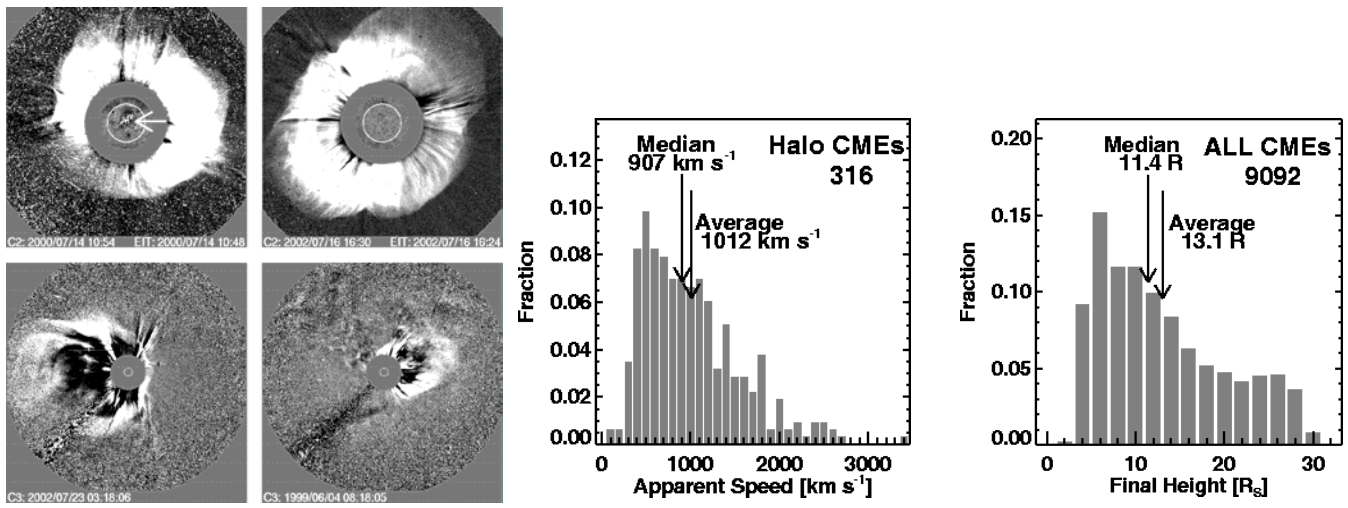

Figure 5. (left) Four examples of halo CMEs (clockwise): front-side full halo, backside full halo, asymmetric halo, and partial halo. (middle) Speed distribution of halo CMEs. Note that their average speed is twice as large as the average speed of the general population. (right) Distribution of the heights of CME leading edges before they faded to the background level. The last bin represents the outer edge of the field of view of the SOHO coronagraphs. Note the second bump between 20 and 30 Rs. These are the CMEs that are likely to cause serious disturbances in the heliosphere.

2.3 Halo CMEs

CMEs which appear to surround the occulting disk of the observing coronagraph are known as halo CMEs (Howard et al. 1982). Despite their discovery in the early 1980s, halo CMEs remained just a novelty in the pre-SOHO era. Now they have proved to be quite prevalent with immense consequence to geospace (Webb et al., 2000; St. Cyr et al., 2000; Webb, 2002; Gopalswamy et al., 2003a; Michalek et al., 2003; Yashiro et al., 2004). Figure 5 (left) shows examples of halo CMEs. The top two are full symmetric halos. The bottom-left is an asymmetric full halo. The bottom right is a partial halo. The asymmetric and partial halo CMEs are caused by solar eruptions occurring close to the limb, whereas the full halos are due to eruptions close to the disk center (front or backside). Coronal images (such as the SOHO/EIT difference images in Fig 5) are needed to decide which way the CMEs are heading. Only about 10% of CMEs reach 1 AU to be detected above the background level (see Fig. 5, right); most of these must be wide events (Gopalswamy, 2004a). Only ~3% of CMEs are observed as full halo CMEs (width = 360 deg, see Fig. 1), which are faster on the average (~1000 km/s, see Fig. 5, middle). When front-sided, these CMEs can directly impact Earth causing geomagnetic storms, provided the magnetic field contained in the CMEs have a southward component.

2.4 CMEs and Geoeffectiveness

For a CME to be geoeffective it needs to originate from close to the solar disk center and it has to possess southward component of the magnetic field for efficient reconnection with Earth's magnetic field to produce geomagnetic storms. Several statistical studies have shown that the CME speed and the strength of the magnetic field it contains primarily decide the intensity of the geomagnetic storms (as measured by the Dst index). The CMEs near the Sun propagate through the interplanetary medium, slow down somewhat, and then are detected in the solar wind by in situ observations (Gosling, 1993). Most of these CMEs have a flux rope structure, which ensures a southward component of the magnetic field and hence produce geomagnetic storms (see, e.g., Huttunen et al. 2005). Occasionally CMEs arrive at Earth with very high inclination resulting in a very intense storm (when the magnetic field is fully southward) or no storm at all (when the magnetic field is fully northward). Apart from these rare cases, it can be said that most of the large geomagnetic storms ($|Dst| > 100$ nT) are caused by Earth-directed CMEs (Gopalswamy et al. 2005b).

Figure 6 shows the properties of SOHO CMEs associated with large geomagnetic storms that occurred during 1996-2003. Clearly, the geoeffective CMEs are faster and wider on the average, very similar to the distribution of halo CMEs. In fact, the majority of the geoeffective CMEs are halo CMEs (see Fig. 6 middle). The longitude distribution shows that most of the CMEs originate from close to the disk center, with a small bias to the western hemisphere. Thus, coronagraphs select the faster and wider CMEs that are most likely to impact Earth. It must be pointed out that coronal holes on the Sun produce high speed solar wind, which can also cause geomagnetic storms, but generally of lower intensity. During 1996-2003, there were only three such storms with intensity barely exceeding 100 nT. However, weaker storms ($|Dst| < 100$ nT) related to coronal holes are more frequent and can cause severe space weather effects such as accelerating electrons in the magnetosphere.
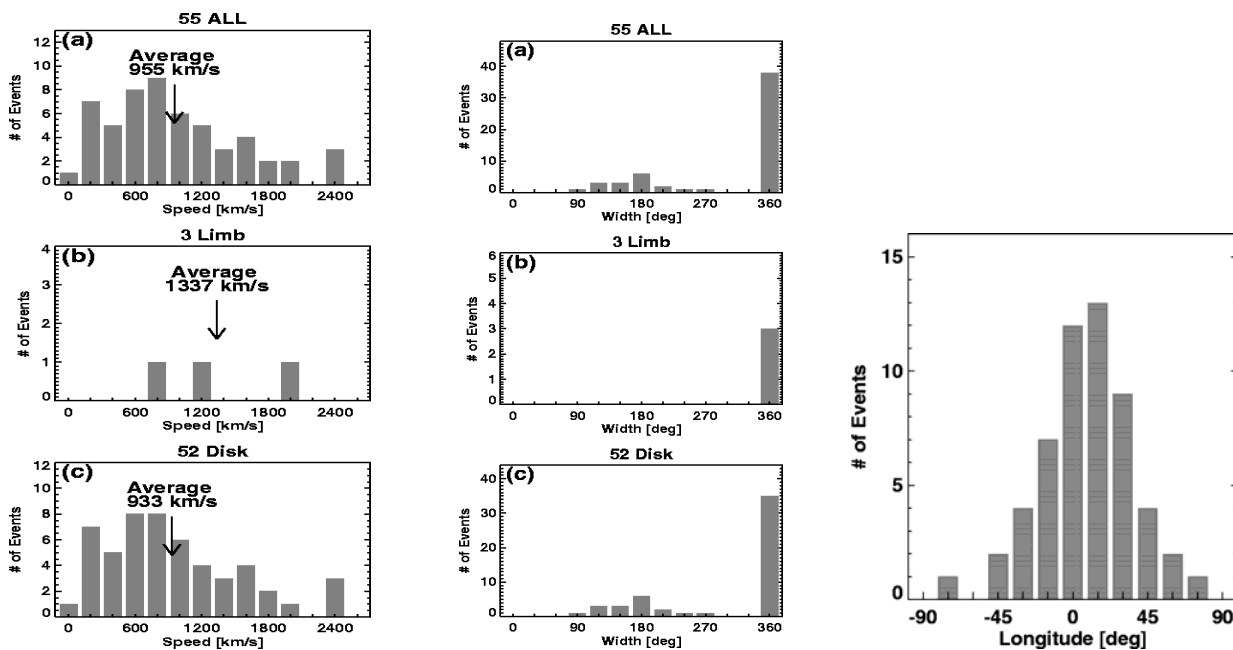

Figure 6. Properties of SOHO CMEs associated with the intense geomagnetic storms: speed (left), width (middle), and eruption longitudes (right). 55 events with clear CME identification are included in the statistics.

In addition to Earth-impacting CMEs, one has also to worry about the asymmetric halos and partial halos in which the plasma does not arrive, but the shock does. Depending on the angle between the Sun-Earth line and the heliographic location of the eruption, the shock with its sheath or just the shock might arrive at Earth. These cases are generally less geoeffective: if the magnetic field in the shock sheath contains southward component, an intense geomagnetic storms may ensue. The arrival of the shock at the magnetosphere also causes sudden commencement, and if strong enough, the shocks arriving at 1 AU often have locally accelerated energetic

particles (Rao et al. 1967). Figure 7 shows two such CMEs originating from close to the limb. The east limb event produced a moderate geomagnetic storm, while the west-limb CME resulted in a strong geomagnetic storm because of the sheath field.
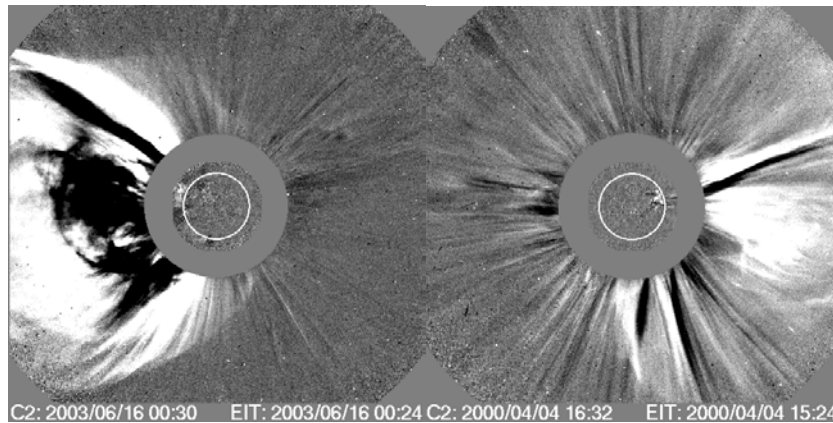

Figure 7. (left) An east limb CME (2003 June 16; speed of 2053 km/s) as observed by SOHO/LASCO. This CME produced a moderate geomagnetic storm (Dst = - 145 nT). (right) A west limb CME (2000 April 4; speed of 1188 km/s), which produced an intense geomagnetic storm (Dst = -321 nT). In both cases, a nearest available difference image from SOHO/EIT is superposed to show that the eruption occurred close to the limb.
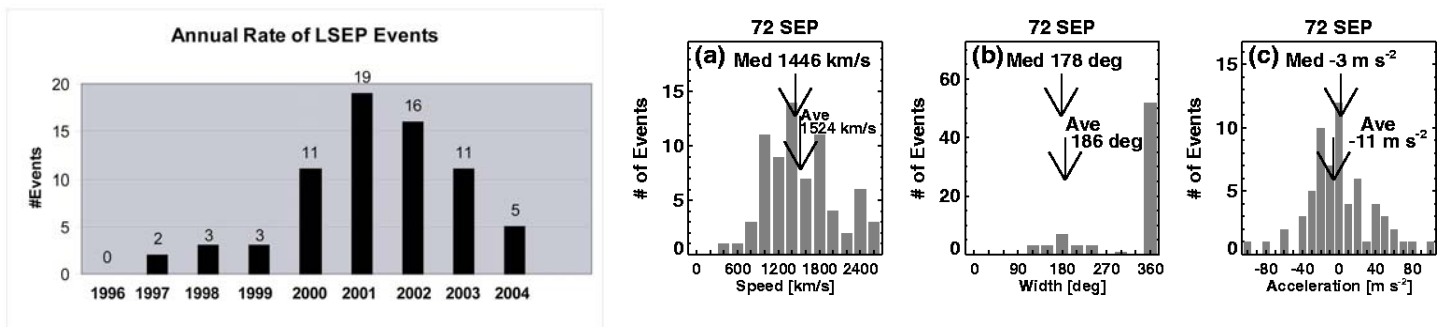

Figure 8. (left) Annual number of large solar energetic particle (LSEP) events from 1996-2004. The maximum number of events occurred around the solar maximum (2000-2003), averaging about 15 events per year. (right) Distributions of speed, width, and acceleration of LSEP-associated CMEs from SOHO/LASCO. The average (Ave) and median (Med) values of the distribution are marked. The average/median values of the width distribution are based on the non-halos. Most (~70%) CMEs are full halos.

2.5 Solar Energetic Particles

If the speed of the CMEs exceeds the local Alfven speed in the corona and interplanetary (IP) medium they can drive shocks, which can accelerate electrons and ions, generally known as solar energetic particles (SEPs). Such CMEs are sometimes referred to be SEPeffective. The close association between SEP events and CMEs first pointed out by Kahler, Hildner, van Hollebeke, et al. (1978) implies that SEPs are accelerated by CME-driven shocks (Reames, 1999). Observations from remote sensing (EIT, LASCO, SUMER) and *in situ* instruments (ERNE/HED) onboard SOHO have shown this connection in great detail (Torsti et al., 2002, Kocharov and Torsti, 2002). One of the very important discoveries is that large SEP events show a sharp maximum in the He3/He4 abundance at 0.015, a factor of 30 higher than the previously assumed value (Torsti et al. 2003). This result helps understand the blurring of the impulsive-gradual paradigm for SEP events. Here we present a global view of the large SEP events (defined as events with particle intensity exceeding 10 pfu in the >10 MeV energy channel).

About 70 such events were recorded during 1996-2004, most of them occurring around the solar maximum (see Fig. 8). The associated CMEs were fast (average speed ~1500 km/s), wide (mostly full halos) and decelerating (due to coronal drag). LSEP events with ground level enhancements (GLEs) are associated with the fastest of all CMEs (average speed ~2000 km/s, see Gopalswamy et al. 2005c). Figure 9 compares the source regions of SEP- and geoeffective CMEs. The source regions of the SEP-associated CMEs are generally located on the western hemisphere, although occasionally LSEP events do occur from the eastern hemisphere. The source distribution is clearly different from that of the CMEs producing geomagnetic storms. Thus, all front sided fast and wide CMEs are important in deciding the conditions in Earth's space environment. According to NOAA classification of radiation storms, >100 pfu events are definitely hazardous because they (i) cause elevated radiation risk event to passengers and crew in high-flying aircraft at high latitudes, (ii) cause single event upsets in satellites, and (iii) affect HF propagation through the polar regions and navigation at polar cap locations. These effects become dramatically serious including impact on astronauts as the SEP intensity crosses 10^3, 10^4, and 10^5 pfu. Thus one can see that all the large-circle events in Fig. 9 (right) are important for space weather purposes. One important result from SOHO is that the high-intensity events occur from active regions that are copious CME producers. In a vast majority of these high-intensity events, the shocks responsible for SEPs seem to be propagating either through the preceding CMEs or their aftermath, posing interesting challenges to particle acceleration theories (Gopalswamy et al., 2004; Li and Zank, 2005). Emslie et al. (2004) have shown that the CME kinetic energy is the largest component in the energy budget of an eruption. As much as 10% of the CME kinetic energy could go into solar energetic particles, suggesting that the CME-driven shocks are very efficient particle accelerators.
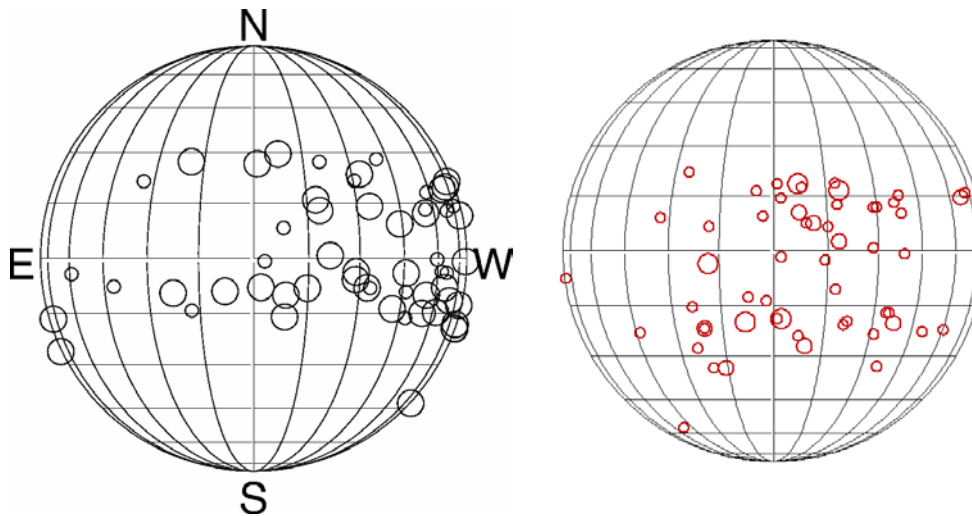

Figure 9. Heliographic locations of SEP-effective CMEs (left) (large circles: >50 pfu events; small circles: <50 pfu events) and Geoeffective CMEs (right) (small, medium, and large circles indicating storms with -100 nT > Dst > -200 nT, -300 nT < Dst < -200 nT, and Dst < -300 nT, respectively) for solar cycle 23. Clearly, the source distributions are different. Both have a western-hemispheric preference, but the SEP-effective events are mostly on the western hemisphere because they are magnetically well-connected to Earth.

2.6 CMEs and Type II Radio Bursts

One of the important contributions of SOHO for understanding the relation between CMEs and type II radio bursts is the identification of solar sources using EUV observations. The coronal dimming phenomenon (see e.g., Zarro et al. 1999) and EUV waves (Thompson et al., 1999) associated with solar eruptions have decisively shown the disk signature of CMEs. While the associated white-light signatures may not be possible due to the presence of coronagraph occulting disk, the EUV signatures clearly identify the large-scale eruption. The dimming and wave signatures are typically larger than the active region from which the eruption originates. This has rendered the existence of CMEless type II bursts (Sheeley et al. 1984; Kahler et al., 1984) questionable. The CMEless type II burst was a strong argument favoring the flares blast waves as the source of metric type II

bursts (see, e.g., Classen and Aurass, 2002). In fact, SOHO has found that there are no CMEless type II bursts (Gopalswamy et al., 2001a), confirming an earlier result by Cliver et al. (1999) from pre-SOHO data. It appears that the type II bursts in various wavelength domains are organized by the kinetic energy of the CMEs: the metric type II bursts (confined to a heliocentric distance of ~2 Rs) are associated with CMEs with above-average kinetic energy. Type II bursts extending to at least the decameter-hectometric (DH) wavelengths (heliocentric distance beyond 2 Rs) are associated with CMEs of moderate kinetic energy. On the other hand type II bursts having counterparts in the metric and DH domains and extending to kilometric wavelengths (bursts over the entire Sun-Earth distance, 2-214 Rs) are associated with CMEs of the largest energy (Gopalswamy et al., 2005d). This hierarchical relationship between CMEs and type II bursts supports a unified approach to all type II bursts as a CME-related phenomenon. Interestingly, most of the SEP events were associated with these m-to-km type II bursts, because the same CME-driven shock accelerates both ions and electrons. The minor difference between the SEP and m-to-km stems from the fact that SEPs need to be well-connected to Earth, whereas the radio emission is widely beamed. Observing the m-to-km type II bursts and the associated CMEs can identify and provide advanced warning on SEPs and energetic plasmas propagating to other destinations in the heliosphere considered for future exploration.

3. CME Interaction
The combination of CME data from SOHO and WAVES (Bougeret et al., 1995) radio data from the Wind spacecraft helped identify the interaction between CMEs. In the white light data, when a fast CME is viewed overtaking a slow CME from the same solar source or a neighboring solar source, often an radio emission is detected in the radio dynamic spectrum (a plot of radio intensity in the frequency-time plane). If such an interaction results in a single resultant CME, the process is referred to as "CME cannibalism" (Gopalswamy et al. 2001c). Fig. 10 shows an example. Two CMEs can be seen distinctly in the first SOHO image (top left). CME 2 was very fast (2657 km/s) approaching a slower CME1 (1000 km/s), with its inner core (CORE1) moving at a speed of ~700 km/s. In the second SOHO image, the CMEs are very close to each other, when the sudden enhancement in radio takes place (see the middle panel between 21:00 and 22:00 UT). The height-time plot in the bottom panel also shows the proximity of the CMEs at the time of the radio enhancement (marked by the two vertical dashed lines). Both the SOHO images in the top panels and the height-time plots indicate that the interaction occurs at a heliocentric distance of ~20 Rs. This is consistent with the frequency of the radio enhancement (starting at 2-3 MHz), which is the plasma frequency of the corona at a distance of about 20 Rs. The shock ahead of CME2 produces normal type II radio emission until it encounters CME1 to produce the enhancement. The mechanism of enhancement is as follows: when the shock of CME2 passes through the high density of CME1, it encounters a region of low Alfven speed (inversely proportional to square-root of density) and hence its Mach number increases temporarily. A high Mach number shock accelerates more electrons resulting in the enhanced radio emission. There may be other mechanisms that boost the efficiency of shock acceleration depending on the magnetic topology of the preceding CME and the turbulence in its aftermath.

The CME interaction is also relevant for SEPs because the same shock accelerates electrons and ions. It was found that whenever an SEP-producing CME is preceded by another CME from the same active region, the resulting particle intensity is higher than in the case with no preceding CMEs (Gopalswamy et al. 2002, 2003a, 2004). In addition, the large scatter in the plot between CME speed and SEP intensity (Kahler, 2001) is significantly reduced when the interacting and non-interacting cases are considered separately. The properties of the preceding CMEs indicate that they have above-average speeds, suggesting that they can also drive shocks, which in turn could accelerate seed particles for the following stronger shock. Presence of seed particles seems to make a difference in the resulting intensity of the SEP events (Kahler, 2001). Another possibility is the flares preceding the main SEP event. These flares may produce seed particles that may influence the composition of resulting SEP events (Mason et al., 1999).
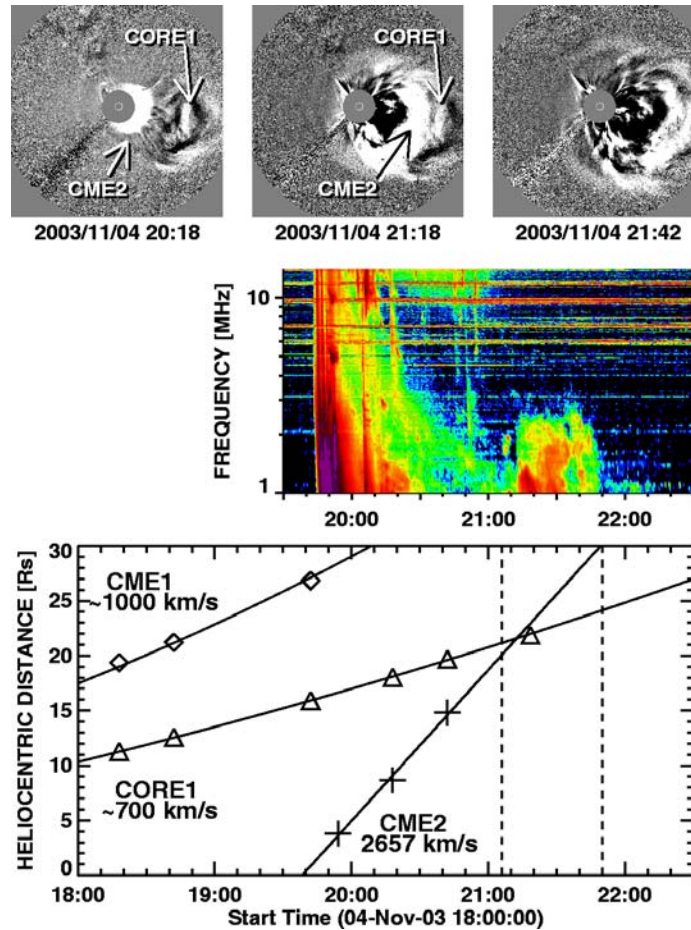
Figure 10. Interaction between two CMEs (top panel) and the corresponding radio enhancement (2-3 MHz). The bottom panel shows the height-time plots of the two CMEs (CME1, CME2) and the inner core of CME1 (CORE1). The two vertical dashed lines mark the interval of radio enhancement (from Gopalswamy, 2004b).

4. CME-Solar Wind Interaction

IP shocks generally decelerate before arriving at 1 AU due to momentum transfer to the solar wind (e.g., Pinter, 1973). Quantifying the deceleration became possible when ICMEs in the IP medium and their counterparts near are compared (Lyndsay et al., 1999; Gopalswamy et al., 2000a; 2001b). Such an analysis resulted in a simple estimate for the interplanetary CME acceleration (a) based on the initial speed (u) of CMEs:

$$a = 2.193 - 0.0054\,u. \quad (1)$$

This relation can be used to predict the arrival time of CMEs at 1 AU and their expected speed (Gopalswamy et al. 2001b). This empirical CME arrival (ECA) model was extended to an empirical shock arrival (ESA) model based on the piston-shock relationship between CMEs and shocks at 1 AU. This model is applicable only to those CMEs which directly impact Earth (so they come as CME-shock pairs). CMEs not directly impacting may also produce a shock signature at 1 AU, but these shocks are generally the flanks of shocks propagating orthogonal to the Sun-Earth line. The model may be used if the input speed is the earthward component of the CME speed. The ESA model can be approximated by a simple formula for faster CMEs (>400 km/s) (see Gopalswamy et al.2005a) connecting the Sun-Earth transit time (T) to the CME speed near the Sun (u):

$$T = A.B^u + C; \; A=151.002, B=0.998625, \text{ and } C=11.5981 \quad (2)$$

Equation (2) predicts that the CME speed has to be ~4300 km/s if the shock has to arrive at 1 AU in half a day. Figure 11 shows a plot of this model with a set of extreme shock arrival times (< 30 h) detected or inferred since

9

the first solar eruption observed by Carrington (1860) and Hodgson (1860). For most of the pre-SOHO events there is no CME observation (CMEs were discovered only in 1971), so we have inferred the CME speeds for these events using equation (11). SOHO contributed two events to this list of historical extreme events (2003 October 28 and 29) during the Halloween 2003 storms (Gopalswamy et al., 2005a). Figure 11 also shows how prevalent the fast CMEs are, indicating that the number of CMEs with speeds exceeding 2000 km/s falls precipitously. This suggests that even the fastest solar shock may take about half a day to arrive at Earth (see equation 2). The accuracy of the prediction of 1 AU travel time can be improved by considering the interaction of CMEs with other CMEs (Manoharan et al., 2004) and by removing the projection effects using a cone model for the earth-directed CMEs (Michalek et al. 2003; Xie et al., 2004).
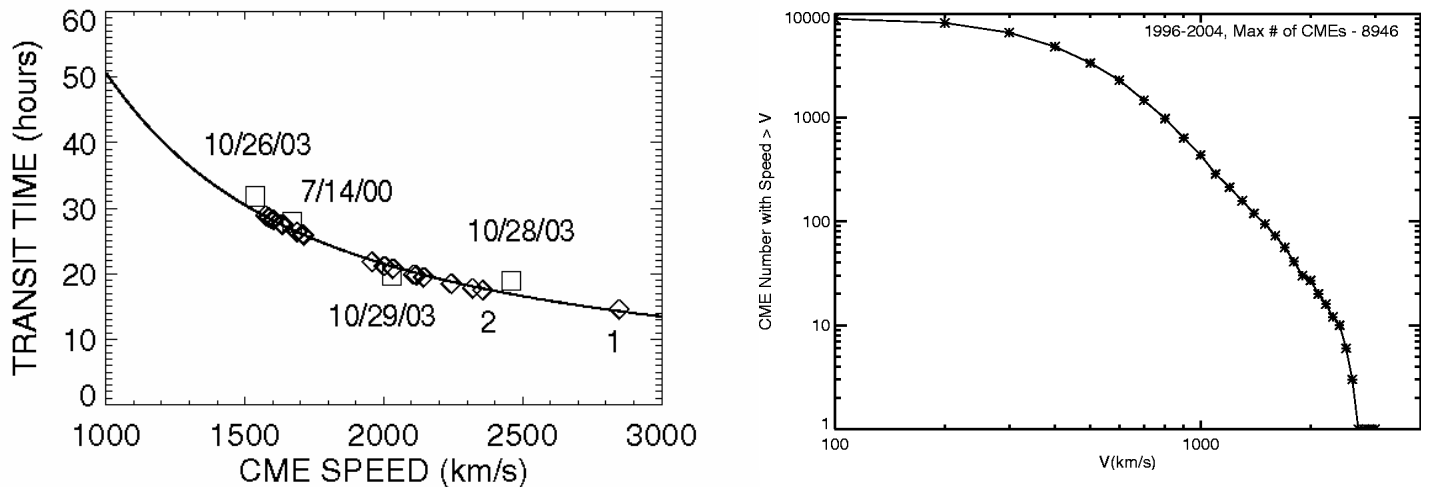

Figure 11. (left) The ESA model (solid curve) for the Sun-Earth transit time of CME-driven shocks with four fastest shocks associated with SOHO CMEs (open squares). The diamonds represent historical (since 1859) fast-transit shocks (T < 30 h). The CME speeds for the historical events were inferred from equation (2). The two fastest shocks are: August 4, 1972 event marked 1 and the Carrington event of 1859 September 1, marked 2). SOHO contributed two events to this list of extreme events (2003 October 28 and 29). The famous Bastille Day event (2000 July 14) is also shown for comparison. (right) The distribution of SOHO CMEs above various speeds, showing that the number of CMEs with speeds exceeding 2000 km/s falls precipitously.

5. Detection of shocks near the Sun

Traditionally, metric type II bursts provided the primary means of detecting shocks associated with solar eruptions. It has been difficult to detect shock waves from white light observations (Vourlidas et al., 2002). The circular wave-like outer structure of halo CMEs may be a manifestation of the shocks because the central CME may be blocked from view by the occulting disk of the coronagraph (Sheeley et al. 1999). When the shocks travel into the IP medium, the radio emission in the DH and km wavelengths again indicates shocks in the IP medium. When the shocks arrive at spacecraft near Earth, both radio emission and the shock can be detected in situ. SOHO's proton monitor detects the IP shocks at L1 and a catalog is maintained. SOHO/UVCS has been useful in detecting shocks near the using spectral in the UVCS emission line profiles and intensities (Raymond *et al.* 2000; Mancuso *et al.* 2002). UVCS spectral observations have also been useful in clarifying the relationship between CMEs and shocks responsible for type II bursts by measuring the density in the pre-event (upstream) corona (Mancuso and Raymond, 2004). Another possible shock signature is the EIT brow waves (see Gopalswamy, 2000; Gopalswamy et al. 2001a; Biesecker et al. 2002). These waves are in general asymmetric with respect to the active region of origin (the "eye"), convex towards the equator (Gopalswamy and Thompson, 2000). This has been suggested to be the occasional sightings of the shock, while the common EIT waves, which are symmetric around the active region of origin and may be the fast-mode MHD waves (see Mann et al., 1999). Although the information has been piece-meal, SOHO has made a significant contribution towards a better understanding of CME-driven shocks.

6. Concluding remarks

We have mainly concentrated on the CMEs and their varied consequences in the heliosphere and geospace. Because SOHO has observed CMEs almost over a solar cycle, we have an extensive data set to fully understand the CME phenomenon. We understand the propagation and heliospheric impact of CMEs rather well, but the origin of the CMEs is still not well understood. Inner coronal imagers of SOHO such as EIT, CDS, and SUMER have provided a number of clues, but still we are unable to predict which regions will erupt. Several processes such as magnetic shear, flux cancellation, and flux emergence are considered as triggers for the eruption. Although we understand the global field of the Sun over 11 and 22 year periods, we are not in a position to predict the emergence of active regions. But several studies have been carried out in this direction using data from SOHO/MDI, which we have not discussed due to space limitations. However, we must point a few important results. The stunning discovery that the emergence active regions can be routinely detected using helioseismic technique has greatly enhanced our ability to watch for potential eruptive regions (Lindsey and Braun, 2000). Images of sound speed in the solar convection zone obtained from the SOHO/MDI shows enhancement within a day before the active region appeared on the solar surface (Kosovichev et al. 2002). Probing deeper into the convection zone seems to be sure way for the early detection of emerging active regions. The wealth of data acquired by SOHO so far and the continued observations will form a gold mine, which is highly likely to contribute to the knowledge on Sun and the heliosphere.

References

Biesecker, D. et al., Astrophys. J., 569, 1009, 2002
Bougeret, J.-L. et al., Space Sci. Rev., 71, 231, 1995.
Brueckner, G.E. et al., Sol. Phys., 162, 357, 1995.
Carrington, R. C., MNRAS, 20, 13, 1860.
Classen, H. T. and Aurass, H. Astron. Astrophys., 384, 1098, 2002.
Cliver, E. W., Webb, D. F., and Howard, R. A., Solar Phys., 187, 89, 1999.
Cliver, E. W. and L. Svalgaard, Solar Phys., 224, 407, 2004.
Gopalswamy, N., Radio Astronomy at Long Wavelengths, Geophysical Monograph. 119, AGU, 123, 2000.
Gopalswamy, N. in "The Sun and the Heliosphere as an Integrated system", ASSL series, edited by G. Poletto and S. Suess, KLUWER/Boston, Chapter 8, p. 201, 2004a.
Gopalswamy, N., Interplanetary radio bursts, in "Solar and Space Weather Radiophysics" edited by D. E. Gary and C. O. Keller, Kluwer, Boston, chapter 15, p.305, 2004b.
Gopalswamy, N. and Thompson, B. J., 2000, JASTP, 62, 1457
Gopalswamy, N. et al., Geophys. Res. Lett., 27, 145, 2000a.
Gopalswamy, N., Kaiser, M. L., Sato, J., and Pick, M., in High Energy Solar Physics, Ed. R. Ramaty & N. Mandzhavidze, PASP Conf Ser., vol. 206, p. 355, 2000b.
Gopalswamy, N., Lara, A., Kaiser, M. L., and Bougeret, J.-L., J. Geo-phys. Res. 106, 25261, 2001a
Gopalswamy, N. et al., J. Geophys. Res., 106, 29207, 2001b.
Gopalswamy, N., Yashiro, S., Kaiser, M. L., Howard, R. A., Bougeret, J.-L., Astrophys. J. 548, L91-L94, 2001c
Gopalswamy, N., Yashiro, S., Michalek, G., Kaiser, M. L., Howard, R. A., Reames, D. V., Leske, R., and von Rosenvinge, T, Astrophys. J., 572, L103-L107, 2002.
Gopalswamy, N.; Lara, A.; Yashiro, S.; Nunes, S., Howard, R. A., In: Solar variability as an input to the Earth's environment. Ed.: A. Wilson. ESA SP-535, Noordwijk: ESA Publications Division, p. 403, 2003a
Gopalswamy, N., Lara, A., Yashiro, S., and Howard, R. A., Astrophys. J., 598, L63, 2003b
Gopalswamy, N. et al., Geophys. Res. Lett., 30(12), SEP 3-1, 2003c.
Gopalswamy, N., Yashiro, S., Krucker, S., Stenborg, G., and Howard, R. A, J. Geophys. Res. 109, 12105, 2004
Gopalswamy, N., S. Yashiro, Y. Liu, G. Michalek, A. Vourlidas, M. L. Kaiser, and R. A. Howard , J. Geophys. Res., in press, 2005a

Gopalswamy, N., S. Yashiro, G. Michalek, H. Xie, R. Lepping, and R. A. Howard, R. A., Geophys. Res. Lett., 32 (12), CiteID L12S09, 2005b

Gopalswamy, N., H. Xie, S. Yashiro, and I. Usoskin, 29th ICRC Conference, in press, 2005c.

Gopalswamy, N., E. Aguilar-Rodriguez, S. Yashiro, S. Nunes, M. L. Kaiser, and R. A. Howard, J. Geophys. Res., in press, 2005d

Gosling, J. T., J. Geophys. Res., 98, 18937, 1993.

Hildner, E. et al., Solar Phys., 48, 127, 1976

Hodgson, R., MNRAS, 20, 15, 1860.

Howard, R. A., D. J. Michels, N. R. Sheeley, N. R., Jr., M. J. Koomen, Astrophys. J. 263, L101-L104, 1982.

Huttunen, K. E. J., R. Schwenn, V. Bothmer, H. E. J. Koskinen, Ann.Geophys., 23, 625, 2005.

Kahler, S. W., J. Geophys. Res., 106, 20947, 2001.

Kahler, S.W.,Hildner, E. and van Hollebeke, M. A. I., Solar Phys., 57, 429, 1978.

Kahler, S., Sheeley, N. R., Jr., Howard, R. A., Michels, D. J., Koomen, M. J., Solar Phys., 93, 133, 1984

Kocharov, L., and Torsti, J., Solar Phys., 207, 149, 2002.

Kosovichev, A., Duvall, T., Birch, A., Gizon, L., Scherrer, P, Zhao, J., Adv. Space Res., 29, 1899, 2002.

Lara, A., N. Gopalswamy, R. Caballero-Lopez, S.Yashiro, and J. Valdes-Galicia, Astrophys. J., 625, 441, 2005.

Li, G. and G. P. Zank, 29th ICRC Conference, Pune, in press, 2005.

Lindsay, G., J. G. Luhmann, C. T. Russell, and J. T. Gosling, J. Geophys. Res., 104, 12515, 1999.

Lindsey, C. and D. C. Braun, Science, 287, 5459, 2000

Mancuso, S., Raymond, J. C., Kohl, J., Ko, Y.-K., Uzzo, M., and Wu, R., Astron. Astrophys., 383, 267, 2002.

Mancuso, S. and J. C. Raymond, Astron. Astrophys., 413, 363-371, 2004.

Mann, G. A., Klassen, Estel, C., and Thompson, B. J. Proc. of 8th SOHO Workshop, Edited by J.-C. Vial and B. Kaldeich-Schmann. 477, 1999.

Manoharan, P. K., Gopalswamy, N., Lara, A. and Yashiro, S., 2004, J Geophys. Res., 109, A06109, 2004.

Mason, G. M., Mazur, J. E., and Dwyer, J. R., Astrophys. J., 525, L133, 1999.

Michalek, G., Gopalswamy, N. and Yashiro, S., Astrophys. J., 584, 472, 2003.

Newkirk, G., Hundhausen, A. J. and Pizzo, V., J. Geophys. Res., 86, 5387, 1981

Pinter, S., Nature Phys. Sci. 243, 96, 1973.

Raymond, J. C., Thompson, B. J., St. Cyr, O. C., Gopalswamy, N., Kahler, S., Kaiser, M., Lara, A., Ciaravella, A., Romoli, M., and O'Neal, R., Geophys. Res. Lett., 27, 1493, 2000.

Reames, D. V., Space Sci. Rev., 90, 413, 1999.

Sheeley, N. R., Howard, R. A., Michels, D. J., Robinson, R. D., Koomen, M. J., and Stewart, R. T. Astrophys. J., 279, 839, 1984.

Sheeley, N. R., J. H. Walters, Y.-M.Wang, and R. A. Howard, J. Geophys. Res., 104, 24739, 1999.

St. Cyr, O. C. et al., J. Geophys. Res., 105, 18169, 2000.

Thompson, B. J. et al., Astrophys. J., 517, L151, 1999.

Torsti, J., Kocharov, L., Laivola, J., Pohjolainen, S., Plunkett, S.P., Thompson, B. J., Kaiser, M. L., Reiner, M. J., Solar Phys., 205, 123, 2002.

Torsti, J., J. Laivola, and L. Kocharov, Astron. Astrophys., 408, L1, 2003.

Tousey, R., Space Res., 13, 713, 1973.

Vourlidas, A.,Wu, S. T.,Wang, A. H., Subramanian, P., and Howard, R. A., Astrophys. J., 598, 1392, 2003.

Rao, U. R., McCracken, K. G., and Bukata, R. P., J. Geophys. Res., 72, 4325, 1967.

Wagner, W. J., 1984, ARA&A, 22, 267

Webb, D. F., Half a Solar Cycle with SOHO, ed. A. Wilson, ESA SP-508, Noordwijk: ESA Publications, p. 409, 2002.

Webb, D. F. and R. A. Howard, J. Geophys. Res., 99, 4201, 1994

Webb, D. F., Cliver, E., Crooker, N. U., St. Cyr, O. C., and Thompson, B. J., J. Geophys. Res., 105, 7491, 2000.

Xie, H. et al., JGR 109, A03109, 2004.

Yashiro, S., N. Gopalswamy, G. Michalek, O.C. St.Cyr, S.P. Plunkett, N.B. Rich, and R.A. Howard, J. Geophys. Res., 109, A7, CiteID A07105, 2004.

Zarro, D., A. Sterling, B. Thompson, H. Hudson, and N. Nitta, Astrophys. J., 520, L139, 1999.